Annals of Biomedical Research
An open access journal
eSciRes
ABR-1-106
Research Article

Sequence-nonspecific Stabilization of Transmembrane Helical Peptide Dimer in Lipid Raft-like Bilayers in Atomistic Simulations. II. Acyl Chain Order-Associated Changes in Lipid-peptide Contacts Concordant with Potential Energy Profiles

Nishizawa M and Nishizawa K*
School of Medical Technology, Teikyo University, Japan

Abstract

Dimerization energetics of two membrane-spanning helical peptides is an important issue to understand dynamics of membrane protein interactions. In a companion paper, we reported our united-atom and all-atom simulation analyses that showed that increases in cholesterol and phospholipids harboring saturated acyl chains in the bilayer stabilize the dimeric state for Ile-rich model transmembrane peptides. In the present paper, we show that in the bilayers with high acyl chain order (raft-like bilayers), lipid acyl chains had simultaneous contacts with both of the dimerized peptides (dual contacts), contributing to the dimer stabilization through Lennard-Jones energy interactions. The ordered acyl chains of the raft-like bilayers caused narrow crossing and tilt angles of peptides, likely assisting formation of the dual contacts. Intriguingly, in the non-raft dioleoylphosphatidylcholine (DOPC) bilayer (low acyl chain order), the lipid-peptide electrostatic energy interaction was in favor of stabilization of the helix *monomer* via better fitting of lipid head groups to monomeric peptides. Thus, both Lennard-Jones and electrostatic interactions are likely to play important roles in the dimeric state stabilization of the helix peptide dimer in a sequence-nonspecific manner in the raft-like bilayers. These findings suggest that switching between distinct modes of lipid-peptide contacts accounts for the differences in the monomer-dimer equilibrium between the raft-like and non-raft lipid membranes.

Key words: Self-association; Lipophobic; Clustering; Solvation; Charmm; GROMOS

Introduction

Dimerization/multimerization of membrane-spanning helix peptides is an essential process in a variety of biological phenomena including protein folding and regulation of cellular signal transduction. It is of biomedical importance to study the effect if lipid composition on the monomer-dimer equilibrium of transmembrane (TM) helical peptides. This issue has mainly been studied with interest in the roles of specific interactions between lipids and peptides [1] as well as of specific residue motifs serving as an dimerization interface [e,g., 2,3]. On the other hand, a relatively limited number of reports have been published on sequence-nonspecific effects of lipid composition either in experimental or computational approach [4,5]. For computational studies, coarse-grained simulations have been extensively used, however, it may often become desirable to gain atomic details to discuss biologically relevant issues. In a companion paper [6], we report our atomistic molecular dynamics (MD) simulation results that showed that bilayers with high acyl chain order (i.e., 1:1:1 and 2:1:1 palmitoyloleoylphosphatidylcholine (POPC)/dipalmitoylphosphatidylcholine (DPPC)/cholesterol bilayer) exhibit a dimeric state-stabilizing effect for poly-Ile model peptides $(Ile)_{21}$ and $I(IV)_{10}$ (Figure 1A). In our comparison between a DOPC bilayer and the 1:1:1 bilayer (which we refer to as the raft-like bilayer), GROMOS^{53A6} and Charmm36 force filed (FF) showed a monomer-dimer equilibrium shift toward the dimeric state with the use of the raft-like bilayer (Figure 3 of [6]) Moreover, potential energy decomposition analyses showed that, for both FFs, both electrostatic and Lennard-Jones interactions are important for the increased stability of the peptide dimers in the raft-like bilayers (Figure 1B and 1C). In the present paper we analyze structural features of lipid-peptide contacts associated with the helix dimer stabilization in the raft-like lipid bilayers.

Methods

MD simulations

All MD simulations and computations of the dimerization free energy ΔG^{dim} based on the potential of mean force (PMF) profiles and of the potential energy decomposition were performed as described in our companion paper [6]. As listed in Table 1, these MD simulations consisted of seven united-atom (UA) GROMOS^{53A6} sets and two all-atom (AA) Charmm36 sets of umbrella sampling simulations. For the potential energy decomposition, we use the terms as we describe in [6], which are the peptide-peptide ($V_{pept\text{-}pept}$), peptide-lipid ($V_{lipid\text{-}pept}$) and lipid-lipid ($V_{lipid\text{-}lipid}$), potential energy, which are further decomposed into the LJ potential energy terms $V^{LJ}_{pept\text{-}pept}$, $V^{LJ}_{lipid\text{-}pept}$ and $V^{LJ}_{lipid\text{-}lipid}$, respectively, and the electrostatic energy terms $V^{Coul}_{pept\text{-}pept}$, $V^{Coul}_{lipid\text{-}pept}$ and $V^{Coul}_{lipid\text{-}lipid}$, respectively.

Distribution of lipid head group atoms in proximity of peptide

We use the term 'proximity' in the analysis of lipid atom distributions near peptides in relation to the lipid-peptide

electrostatic potential energy, whereas we use 'contact' to analyze lipid atom distributions close to the peptides for comparison with the *LJ* potential energy as described in the next section. In both the proximity and contact analyses, our self-made programs prepared with attention to the periodic boundary condition were used.

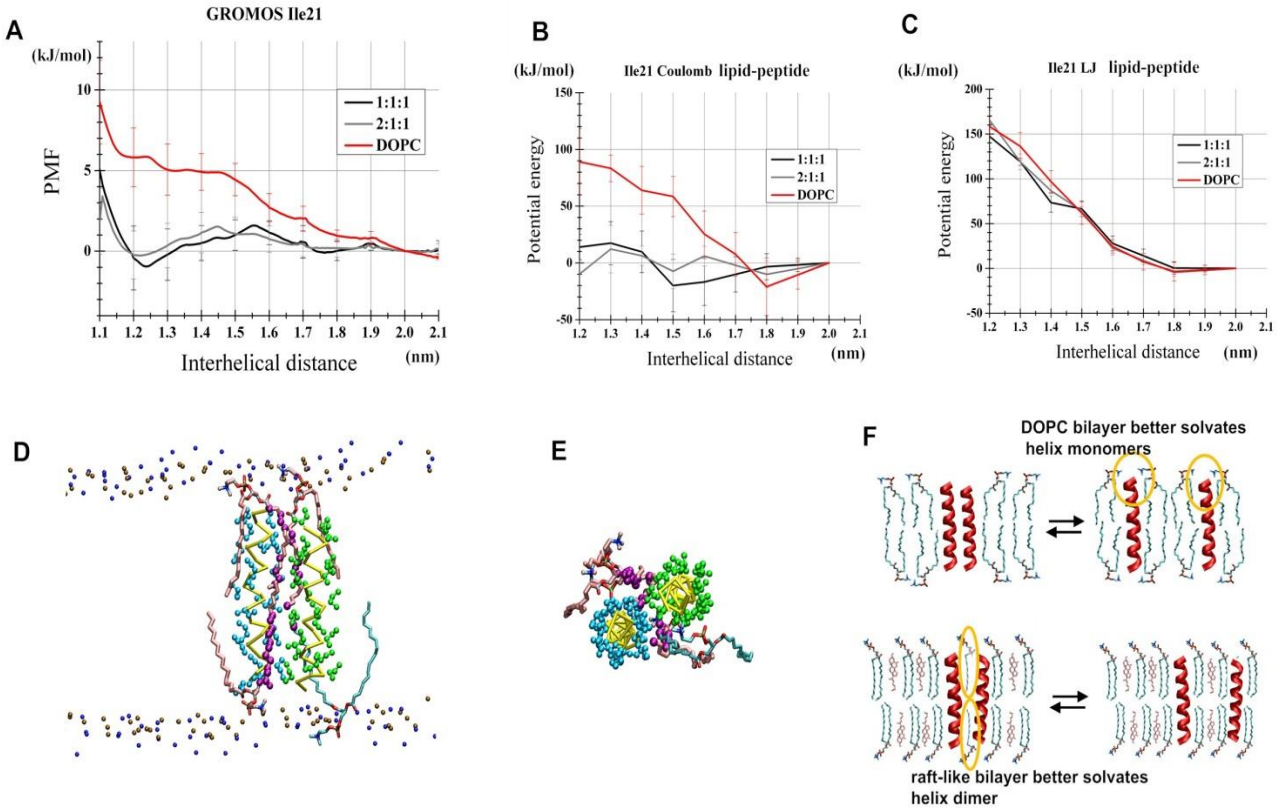

Figure 1: Selected profiles and snapshots of PMF simulations of the poly-Ile ($(Ile)_{21}$) model peptide. (A) PMF profiles obtained from the Gr-Ile_{21}-dopc set (#1 of Table 1) and the Gr-Ile_{21}-1-1-1 set (#2) and the Gr-Ile_{21}-2-1-1 set (#3). (B) Profiles of the electrostatic potential energy component $V^{Coul}_{lipid\text{-}pept}$ between lipid and peptide. (An excerpt from [6].) The results for the #1, 2, and 3 of Table 1 are shown. (C) Profiles of the LJ potential energy component $V^{LJ}_{lipid\text{-}pept}$ between lipid and peptide. (An excerpt from [6].) (D) A timeframe of the Gr-Ile_{21}-1-1-1 set (r=1.3 nm) that showed dually contacting phospholipids (pink licorice representation). The acyl chain atoms showing dual contacts are highlighted in purple spheres. Phospholipid nitrogen and phosphorus atoms are shown as blue and ochre spheres. Yellow bars represent peptide backbone trace. Green and cyan spheres represent Ile side chains. (E) A view from the bottom of the structure presented in (D) but only the lipids with dual contacts are shown for clarity. (F) Schematic drawing summarizing the main findings of this study.

The models of phosphatidylcholine head group used in the GROMOS and the Charmm analyses are shown in Figure 2. For the proximity analysis, the atoms of a phospholipid head group were divided into the three groups: group 1, group 2 and group 3 (Figure 2). As the group 1 largely corresponds to a choline group, for brevity we will refer to the group 1 as the choline group in this study. We also refer to the group 2 and the group 3 as the phosphate (or 'po4') group and the 'glycco' (the glycerol backbone plus carbonyl oxygen) group, respectively. From the GROMOS simulations, the distribution of the group 1 atoms in the proximity of the peptides was analyzed as follows. First, for the i^{th} atom (reference atom) of the group 1, we counted $N_{i\text{-}bb8}$, which represents N_{bb8} of i^{th} (reference) atom, where N_{bb8} is the number of those peptide backbone atoms which were located within 8 Å of the reference atom. Then, we computed 'the proximity index of choline' $S_{choline}$ defined as $S_{choline} = \sum N_{i\text{-}bb8}$, where the sum was taken by scanning the *i* over all atoms (of group 1, in this case), of all phosphatidylcholine molecules in the system. Thus, $S_{choline}$ is an approximate measure of the proximity-weighted density of the choline group of phosphatidylcholine near the peptide backbones. Likewise, S_{po4} and S_{glycco} were defined as the sum of $N_{i\text{-}bb8}$ across the group 2 atoms, and that across the group 3 atoms, respectively. Here, under the GROMOS force field (FF), the peptide backbone atoms (and partial charges) were defined as C_α (0.0), C (0.45), O (-0.45), N (-0.31) and H (0.31). The N-terminus acetyl group (cap) consisted of an UA particle representing CH_3 with no charge, along with C (0.45) and O (-0.45). The C-terminus cap (amino group) consisted of N (-0.83) and two H (0.415) atoms.

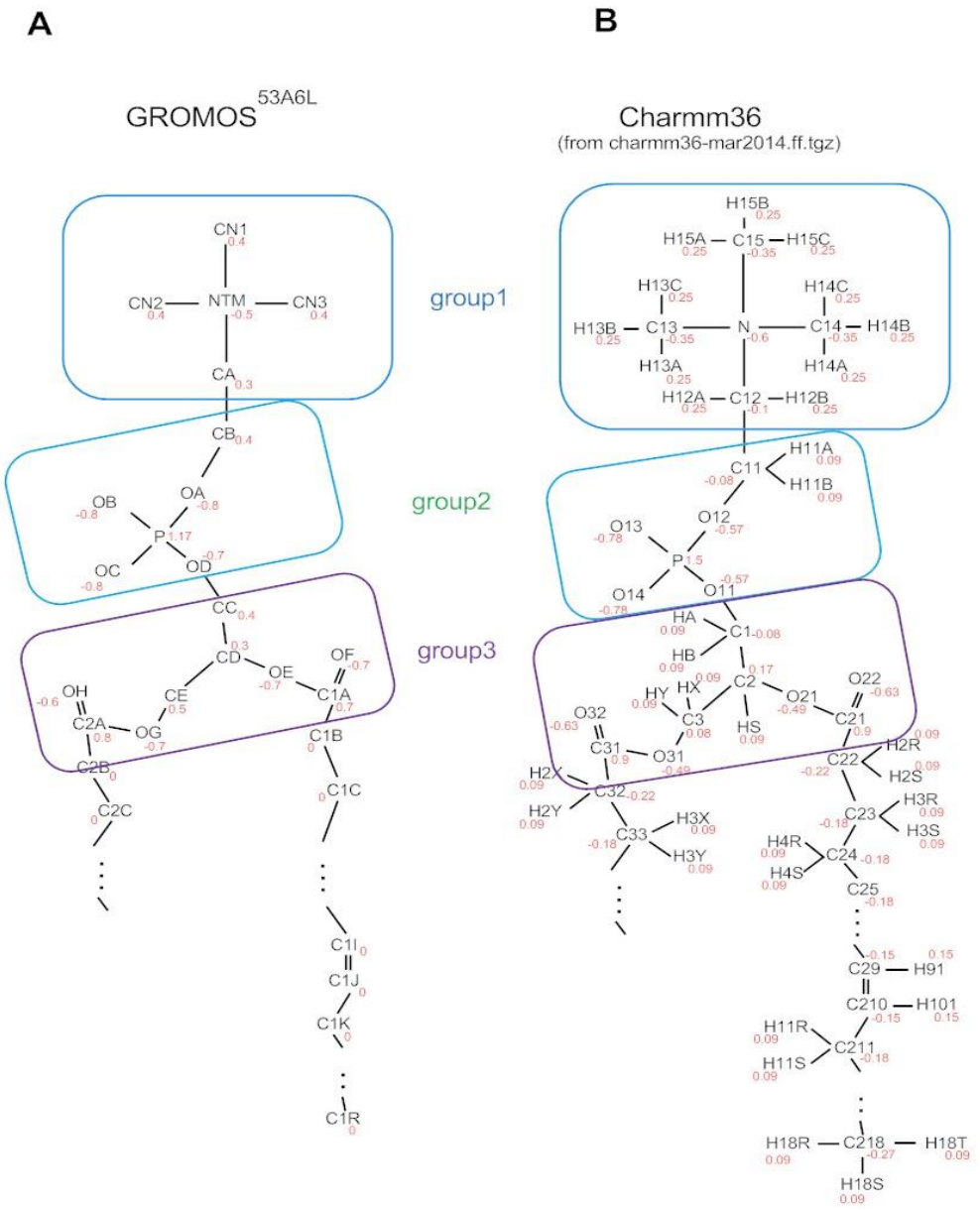

Figure 2: Atom types and atomic electric charges (in elementary charge e) assigned to the head group of POPC under the GROMOS (A) and Charmm (B) parameters.

The proximity indices were similarly defined for the Charmm simulations, with the hydrogen atoms of the phospholipid head groups being excluded from the reference atoms. The hydrogen atoms bonded to the C_α were also excluded in the N_{bb8} analysis. Thus, in the Charmm analyses, the peptide backbone atoms used for the N_{bb8} computation were C_α (0.07), C (0.51), O (-0.51), N (-0.47) and H (0.31) and the two carbon and oxygen atoms of the N-terminus-capping acetyl group (C (-0.27), C (0.51), and O (-0.51),) and the atoms of the C-terminus-capping amino groups (N (-0.62), H (0.3) and H (0.32)).

Counts of lipid atoms contacting with peptides

The distance between a lipid atom and a peptide was defined by the distance between the lipid atom and the peptide atom (excluding the hydrogen atoms of the amino acid sidechains in the Charmm analyses) that was the nearest to the lipid atom. When a lipid atom was located within D_{cutoff} from both of the two peptide molecules, such an atom was regarded as 'a dually-contacting' atom. D_{cutoff} was set at 5 or 6 Å. We let $N_{lip\text{-}atom}^{dual}$ represent the number of the lipid non-hydrogen atoms that had dual contacts to both peptides. We further use $N_{lip\_2\text{-}6\text{-}atom}^{dual}$ and $N_{lip\_7\text{-}11\text{-}atom}^{dual}$, and $N_{lip\_12\text{-}16\text{-}atom}^{dual}$ to represent the number of the dually-contacting carbon atoms among those atoms comprising the lipid acyl chain proximal (C2-C6), middle (C7-C11) and distal (C12-C16) segments, respectively. $N_{lip\_head\text{-}atom}^{dual}$ represents the dually-contacting non-hydrogen atoms/particles of phospholipids head groups, where head groups are defined to be comprised of the phosphorylcholine group and the glycerol backbone including oxygen (ester and carbonyl) atoms as well as the carbon atom,

C1, of the carboxyl group. Likewise, $N_{lip\_choloh\text{-}atom}^{dual}$ and $N_{lip\_cholc\text{-}atom}^{dual}$ represent the dually-contacting atoms of the OH group and of the carbon atoms of cholesterol molecule, respectively.

To count the phospholipid acyl chains in close contact with both peptides, we initially defined N_{acyl}^{dual} that represents the number of acyl chain whose all carbon atoms had dual contacts. We also introduced $N_{acyl\text{-}prox}^{dual}$ and Nacyl-distdual that represent the number of the acyl chains whose all proximal segment (C2-C9) carbon atoms and the distal segment (C9-C16) carbon atoms, respectively, had dual contacts.

Basic structural properties of membranes

In the analysis shown in Tables 7 and 8, 'C-P tilt' represents the angle between the z-axis (i.e., the direction of the bilayer normal) and the vector linking the middle carbon atom of the glycerol backbone to the phosphorus atom of the phosphorylcholine. 'C-N tilt' similarly defined using the vector ending at the nitrogen atom of the choline group. The peptide tilt angle was computed using the program *g_helixorient* of Gromacs that uses the coordinates of four consecutive Cα atoms to define the local direction of helix axis. We represented the helix tilt angle against the z-axis based on the average of the vectors based on the four residue-segments of the C7-C14 segment. The derived average vector was also used for computation of the crossing angle between the two helical peptides.

Results and Discussion

The sets of the PMF measurements and simulation setups used in our companion paper are summarized in Table 1 and selected results are shown in Figure 1A, 1B and 1C. Compared to the sets with the DOPC bilayer (ID #1,6,8 in Table 1), the use of the raft-like bilayers (ID #2,3,7,9) showed a consistent trend of stabilization of the dimeric state relative to the monomeric state as shown by the more negative ΔG^{dim} values. Although the dimerization energy based on MD simulations is highly sensitive to the FF used and UA FFs may tend to have inaccuracy in parameters describing the lipid atom-peptide atom interactions, causing substantial discrepancies from the data with AA FFs [7], our decomposition analysis showed a result consistent between GROMOS and Charmm analyses ([6] and Table 1). That is, for both the lipid-peptide LJ term $V^{LJ}_{lipid\text{-}pept}$ and the lipid-peptide electrostatic energy term $V^{Coul}_{lipid\text{-}pept}$, the profiles showed changes dependent on interhelical distance r, concordant to the PMF profiles. Thus, these results suggested that both the LJ and electrostatic energies are important factors that explain the stabilization of the helices dimer in the raft-like membranes.

ID (#)	System	ΔG^{dim} (± SE) (kJ/mol)	mean (± SE) of $\{V^{LJ}_{lipid\text{-}pept}(1.3) - V^{LJ}_{lipid\text{-}pept}(2.0)\}$ (kJ/mol)	mean (± SE) of $\{V^{Coul}_{lipid\text{-}pept}(1.3) - V^{Coul}_{lipid\text{-}pept}(2.0)\}$ (kJ/mol)
1	Gr-Ile$_{21}$-dopc	0.23 ± 0.56	136.2 ± 15.4	83.3 ± 11.6
2	Gr-Ile$_{21}$-1-1-1	−1.34 ± 0.44	119.1 ± 3.9	17.4 ± 19.0
3	Gr-Ile$_{21}$-2-1-1	−1.22 ± 0.45	119.0 ± 8.8	12.2 ± 20.9
4	Gr-Ile$_{21}$-popc	−0.06 ± 0.69	138.9 ± 17.5	65.2 ± 16.7
5	Gr-Ile$_{21}$-3-1	−0.17 ± 0.75	133.5 ± 8.1	3.0 ± 21.9
6	Gr-IV-dopc	0.42 ± 0.59	114.5 ± 6.0	61.1 ± 12.4
7	Gr-IV-1-1-1	−1.81 ± 0.57	84.6 ± 8.7	−5.0 ± 11.4
	System	**ΔG^{dim} (± SE) (kJ/mol)**	**mean (± SE) of $\{V^{LJ}_{lipid\text{-}pept}(1.3) - V^{LJ}_{lipid\text{-}pept}(1.6)\}$ (kJ/mol)**	**mean (± SE) of $\{V^{Coul}_{lipid\text{-}pept}(1.3) - V^{Coul}_{lipid\text{-}pept}(1.6)\}$ (kJ/mol)**
8	Ch-Ile$_{21}$-dopc	−1.75 ± 0.22	78.1 ± 8.1	−5.2 ± 6.9
9	Ch-Ile$_{21}$-1-1-1	−2.99 ± 0.30	61.8 ± 7.0	−37.5 ± 8.0

Table 1: The dimerization free energy and and the differential of the potential energy terms based on PMF computations[a].

Lipid-peptide electrostatic potential energy associates with the numbers of lipid head group atoms residing in proximity of peptides

How can the lipid-peptide electrostatic potential energy $V^{Coul}_{lipid\text{-}pept}(r)$ become important for the helix dimer stabilization in the raft-like relative to the non-raft bilayers (Figure 1B)? In the GROMOS FF, no atomic charge is assigned to the lipid acyl chain atoms nor the side chain atoms of aliphatic amino acids (Figure 2), and therefore, $V^{Coul}_{lipid\text{-}pept}$ arises solely from interactions between the lipid head groups and the peptide backbones. So, we further decomposed $V^{Coul}_{lipid\text{-}pept}$ into the electrostatic interactions between the peptide backbone and each of the three following groups:

group 1 (similar to the choline group), group 2 (similar to the phosphate group) and group 3 (the glycerol backbone group plus carbonyl oxygen atoms, which will be referred to as 'glycco') (Figure 2). Intriguingly, in combination with the peptide backbone atoms, the group 1 (choline) and, to a modest degree, group 3 (glycerol backbone) were observed to decrease the electrostatic potential energy for the monomeric state (i.e., stabilize the monomeric state) in the DOPC bilayer, relative to the dimeric state (*red line* of Figure 3B and 3D). For the group 2 (phosphate), this trend was no clear (Figure 3C), yet the total lipid-peptide electrostatic potential energy showed a clear stabilizing effect on the monomeric state in the DOPC system (Figure 3A). In contrast, in the raft-like 1:1:1 bilayer, the monomeric (r=1.3 nm) and dimeric (r=2.0 nm) states showed similar levels of the electrostatic energy between the head group (total and groups 1 to 3) and the peptide backbones (black line of Figure 3A, 3B, 3C and 3D). Accordingly, the lipid-peptide electrostatic potential energy value (i.e., $V^{Coul}_{lipid\text{-}pept}$ (r)) at r=2.0 nm (monomeric state) was -419.4 kJ/mol in the raft-like bilayer, which was high (unfavorable) compared to the DOPC bilayer (-502.7 kJ/mol, Table 2). Similar features were observed for the $I(VI)_{10}$ peptide systems (#6 and 7) (Figure 3E, 3F, 3G and 3H). Therefore, the lipid head groups of the DOPC bilayer appeared to assume energetically favorable locations/orientations with respect to the helix monomers, whereas their fitting to the helix dimer was energetically less optimal, destabilizing the helix dimer in the DOPC bilayer. In contrast, in the raft-like bilayers, both $(Ile)_{21}$ and $I(VI)_{10}$ systems showed only small differences in these electrostatic profiles upon dimerization from the monomeric state, suggesting that the electrostatic interactions between the lipid head groups and the peptides do *not destabilize* the helix dimer significantly in the raft-like bilayers. Although to a modest degree, the Charmm systems showed a similar trend; when compared to the 1:1:1 raft-like bilayer system, the DOPC bilayer system showed a relatively high peptide-lipid electrostatic energy at r=1.3 nm (Figure 7F of [6], and Table 3). Comparison between the r=1.3 and 1.6 nm showed that the helix dimer was better stabilized in the 1:1:1 bilayer than in the DOPC bilayer in the Chramm analyses. Taken together, the lipid-peptide electrostatic interaction is likely to act to better stabilize the helix dimer in the raft-like than in the DOPC bilayer.

	Interhelical distance r (nm)		**1.3**	**2.0**
	potential energy/proximity metrics			
Gr-Ile_{21}-dopc (#1)	$V^{Coul}_{lipid\text{-}pept}$ (± SE) (kJ/mol)		−419.5 (± 8.5)	−502.7 (± 10.4)
	proximity index ± SD	$S_{choline}$	464.2 ± 82.3	607.2 ± 97.3
		S_{po4}	569.7 ± 105.9	738.4 ± 136.4
		S_{glycco}	949.7 ± 119.3	1162.3 ± 132.9
		total[b]	1983.7 ± 253.6	2507.9 ± 266.2
Gr-Ile_{21}-1-1-1 (#2)	$V^{Coul}_{lipid\text{-}pept}$ (± SE) (kJ/mol)		−402.0 (± 6.7)	−419.4 (± 17.4)
	proximity index ± SD	$S_{choline}$	426.2 ± 71.4	470.4 ± 65.5
		S_{po4}	534.4 ± 104.8	574.6 ± 93.0
		S_{glycco}	833.8 ± 131.3	894.0 ± 110.1
		total[b]	1794.4 ± 235.4	1939.0 ± 199.4
[a]To represent the ranges of fluctuations, the data of proximity indices are shown with SD. All proximity indices showed significant differences ($p<10^{-69}$) between 1.3 and 2.0 nm. [b] The sum of the proximity indices $S_{choline}$, S_{po4} and S_{glycco}.				

Table 2: Proximity analysis of lipid head group distribution near peptides based on GROMOS simulations[a].

	interhelical distance r (nm)		**1.3**	**1.6**
	potential energy/proximity metrics			
Ch-Ile_{21}-dopc (#8)	$V^{Coul}_{lipid\text{-}pept}$ (± SE) (kJ/mol)		−105.4 (± 5.6)	−100.2 (± 3.4)
	proximity index ± SD	$S_{choline}$	227.9 ± 82.3	234.7 ± 74.6
		S_{po4}	281.8 ± 100.5	285.1 ± 89.9
		S_{glycco}	752.2 ± 187.6	782.0 ± 150.4
		total[b]	1262.0 ± 317.0	1301.8 ± 253.5
Ch-Ile_{21}-1-1-1 (#9)	$V^{Coul}_{lipid\text{-}pept}$ (± SE) (kJ/mol)		−119.9 (± 6.6)	−82.4 (± 2.3)
	proximity index ± SD	$S_{choline}$	219.2 ± 71.2	212.4 ± 68.1
		S_{po4}	270.1 ± 85.5	251.7 ± 79.8

		S_{glycco}	730.2 ± 146.9	729.1 ± 145.8
		total[b]	1219.4 ± 246.9	1193.3 ± 231.0
[a]To represent the ranges of fluctuations, the data of proximity indices are shown with SD. With the exceptions of S_{po4} for the Ch-Ile$_{21}$-dopc set and S_{glycco} of the Ch-Ile$_{21}$-1-1-1 set, all proximity indices and the total showed significant differences ($p < 0.0005$) between 1.3 and 1.6 nm. [b]The sum of the proximity indices $S_{choline}$, S_{po4} and S_{glycco}.				

Table 3: Proximity analysis of lipid head group distribution near peptides based on Charmm simulations[a].

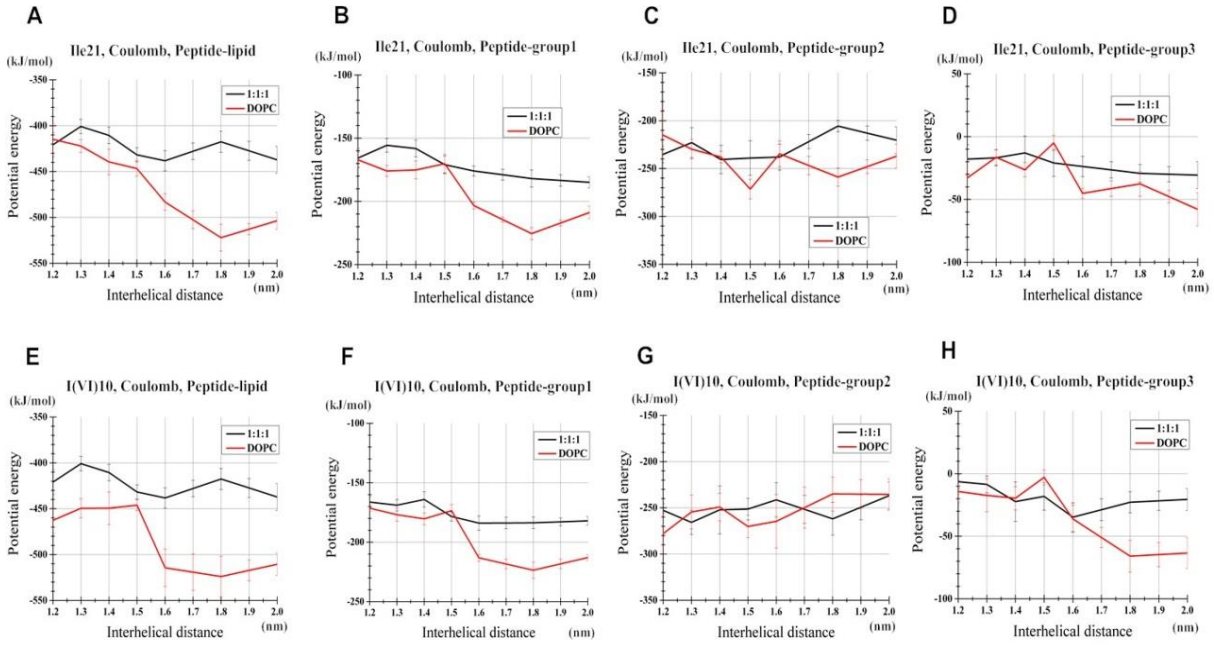

Figure 3: Decomposition analysis of the electrostatic potential energy between the lipids and the peptides. In this figure, the absolute energy values are shown. (A-D) Results for the Gr-Ile$_{21}$-1-1-1 (#2) and Gr-Ile$_{21}$-dopc (#1) runs. (A) The electrostatic potential energy between total lipids and peptides ($V^{Coul}_{lipid\text{-}pept}$). Of note, this term includes cholesterol-peptide electrostatic interaction. (B) $V^{Coul}_{choline\text{-}pept}$, the electrostatic energy between the group 1 atoms (defined in Figure 2) and the peptides. (C) $V^{Coul}_{po4\text{-}pept}$, the electrostatic energy between the group 2 and the peptides. (D) $V^{Coul}_{glycco\text{-}pept}$, the electrostatic energy between the group 3 and the peptides. (E-H) Results on the Gr-IV-1-1-1 (#7) and the Gr-IV-dopc (#6) systems. (E) $V^{Coul}_{lipid\text{-}pept}$, the electrostatic potential energy between total lipids and peptide. (F) $V^{Coul}_{choline\text{-}pept}$, the electrostatic energy between the group 1 and the peptides. (G) $V^{Coul}_{po4\text{-}pept}$, the electrostatic energy between the group 2 and the peptides. (H) $V^{Coul}_{glycco\text{-}pept}$, the electrostatic energy between the group 3 and the peptides.

Lipid-peptide electrostatic interaction change between monomeric and dimeric states and between DOPC and raft-like bilayers: account from lipid atoms residing in proximity of peptides

To gain structural insights into the above results showing the contribution by the lipid-peptide electrostatic interactions to the helical dimer stability in the raft-like bilayer, we counted N_{bb8}, i.e., the number of those peptide backbone atoms that were within 8 Å of each head group (reference) atom (see Method). Then, we summed N_{bb8} over all atoms of the group 1 (Figure 2) to obtain the proximity index $S_{choline}$ for each time frame of simulation runs. As histograms show (Figure 4A), approximately 30 atoms of the group 1 atoms had five or greater N_{bb8} values for the 1:1:1 system, but the corresponding number was higher for the DOPC runs with r=2.0 nm (grey bars, Figure 4D). That is, in accordance with the electrostatic potential energy analysis (Figures 1B, 3B, 3F and [6]), the number of those choline group atoms (reference atoms) which resided in the proximity of the peptides was high for the DOPC/the monomeric peptides simulations (r=2.0 nm) relative to the DOPC/dimeric peptides simulations (r=1.3 nm) (white bars, Figure 4A and 4D). Another important feature was that, between the monomeric and dimeric states, the difference in the number of the head groups residing in the proximity of peptides was small for the 1:1:1 bilayer, compared to the DOPC case (Figure 4A and 4D). The analysis using the proximity index reinforced this conclusion; the $S_{choline}$ value showed a difference of the dimeric state < the monomeric state for the DOPC bilayer while showing a relatively small dimer-*vs.*-monomer difference in the 1:1:1 system (Table 2). Based on the histogram analysis as well as the proximity indices S_{po4} and S_{glycco}, the non-choline head group atoms also showed a trend similar to the case with choline atoms, that is, concordance with the electrostatic potential energy profiles (Figure 4B, 4C, 4E and 4F, Figure

3C, 3D, 3G and 3H, and Table 2). Overall features were similar for the Charmm systems (Table 3).

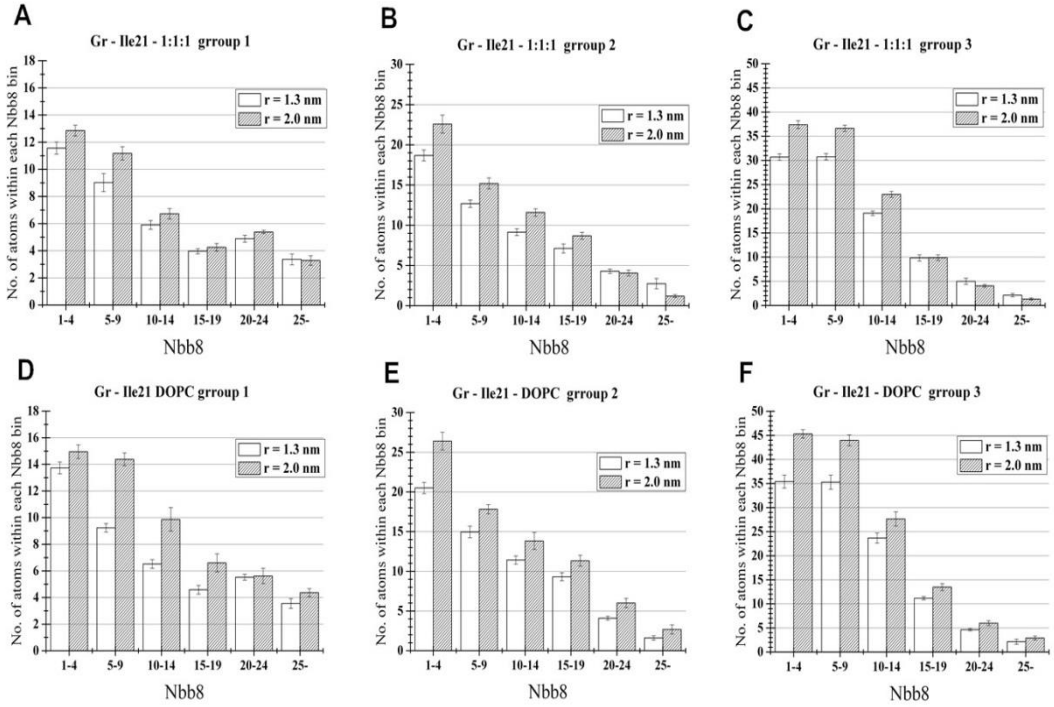

Figure 4: Histograms showing the numbers of the lipid head group atoms that had indicated ranges of N_{bb8}, i.e., the number of the peptide backbone atoms located in the proximity (< 8 Å). (A-C) Results on the Gr-Ile$_{21}$-1-1-1 system (#2). (A) Results for the group 1 (that approximates the choline group) atoms. (B) The group 2 (phosphate group) atoms. (C) The group 3 (glycerol backbone and carbonyl oxygen group) atoms. (D-F) Gr-Ile$_{21}$-dopc system (#1). (D) Results for the group 1 atoms. (E) Results for the group 2 atoms. (F) Results for the group 3 atoms.

Taken together, better fitting of the head group atoms to the peptide monomers is likely to contribute to the lowering the lipid-peptide electrostatic potential energy in the DOPC bilayer, thereby stabilizing the monomeric state. In contrast, for the 1:1:1 raft-like bilayer, the fitting inferred from these proximity indices was similar between the monomeric and the dimeric states (Table 2, i.e., GROMOS sets), or even better in the dimeric state than in the monomeric state (Table 3, i.e., Charmm sets).

The following data supported the impact of the abundance of phospholipid head group atoms in the proximity of the peptides on the lipid-peptide electrostatic potential energy. When the mean of the lipid-peptide electrostatic potential energy $V^{Coul}_{lipid\text{-}pept}(r)$ as well as the proximity indices were computed from 100ns-segments of trajectories and plotted, significant negative correlations of $V^{Coul}_{lipid\text{-}pept}(r)$ with the sum of (and each of $S_{choline}$, $S_{glycerol}$ and S_{po4}) were observed for both r=1.3 and 2.0 nm (Figure 5AB and data not shown). The Charmm set also showed this trend (Figure 5C) findings support the view that abundance of the phospholipid head groups in the proximity of the peptides is an important determinant for the electrostatic potential term and contributes to the helix dimer stability in the raft-like bilayers relative to the non-raft bilayers.

It is not presently clear how such differences in the lipid head group-peptide interactions arise between the DOPC and the 1:1:1 bilayers. One possibility is that in the raft-like bilayer system, cholesterol-phospholipid interaction may restrict the range of motion of the head groups, thereby compromising the fitting of the head groups to the peptides in the monomeric state and negating the monomer-stabilizing effect of this term observed in the DOPC bilayer. In any events, our findings suggest that the electrostatic interaction between the phospholipid head groups-peptides becomes important for the control of the helix monomer-dimer equilibrium. This was unexpectedly significant given that our systems were devoid of charged amino acid residues such as Lys nor lipid head groups with net charges like phosphatidylserine.

Acyl chains simultaneously contacting with both of dimerized peptides are increased in raft-like bilayers relative to non-raft bilayers

Thus, results on $V^{LJ}_{lipid\text{-}pept}(r)$ (Figures 6B, 6E, 7E of [6] and Figure 1C) suggested that the ordered (extended) structures of lipid chains in the raft-like bilayers enable better solvation of the dimeric peptides compared to the chains in the non-raft type bilayers. To address this question, we counted the number of phospholipid acyl chains that were in contact with peptides (i.e., located within D_{cutoff} of peptides). We especially refer to a lipid atom that contacts with both peptides simultaneously as a 'dually-contacting' atom. The number of those acyl chains whose all constituents CH_2 and CH_3 (united) atoms had dual contacts was too small (data not shown). The number, $N_{acyl\text{-}prox}{}^{dual}$, of those acyl chains whose all eight proximal carbon atoms (i.e., C2-C9) had dual contacts (within D_{cutoff}=5 Å) with dimerized peptides (r=1.3

nm) did not show consistent results among the different membranes examined (Table 4). In contrast, when the number ($N_{acyl\text{-}dist}^{dual}$) of those acyl chains that had dual contacts via all carbons of the distal segment (C9-C16) was counted for r=1.3 nm simulations, it was greater for the raft-like (#2, 7 and 9) relative to the non-raft type (#1, 6 and 8) bilayers (Table 4). Both UA (#1, 2, 6 and 7) and AA (#8 and 9) simulations showed this feature. An example of the simulation snapshots showing dual contacts of the lipid distal segments is shown in Figure 1D and 1E. When the definition of contact was loosened to D_{cutoff}=6 Å, the difference between the raft-like and non-raft bilayers was less pronounced, but a similar trend remained (bottom of Table 4). Thus, compared to the non-raft bilayers, the raft-like bilayer systems are likely to allow the acyl chains distal segments to have more dual contacts with the peptides.

When the number of dually-contacting atoms of acyl chains was examined, the proximal (C2-C6) and middle (C7-C11) atoms did not show consistent results in the raft-like system *vs.* the non-raft system comparisons (Table 5). Nonetheless the atoms of the distal segment (C12-C16) showed a consistent trend, that is, as the more ordered the lipid tails were, the greater number of distal segments atoms had dual contacts (Tables 5 and 6), although this trend was not seen between the POPC (#4) and the 3:1 POPC/cholesterol (#5) systems likely because of their small difference in the acyl chain order (Table 6).

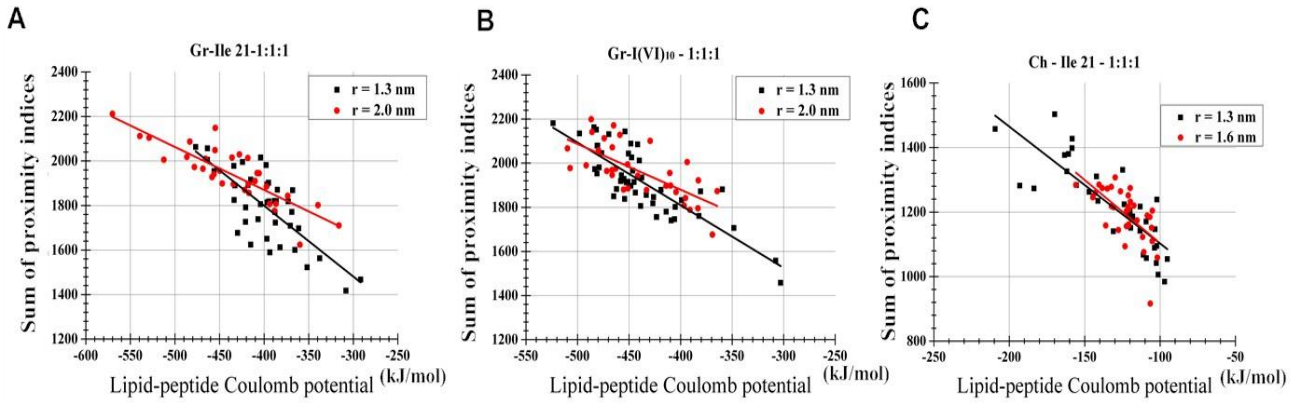

Figure 5: Scatter plot analysis of the lipid-peptide electrostatic energy plotted against the proximity index. Each plot corresponds to a 100 ns segment of the simulation trajectories. Each line represents the linear regression against all data of each of the r=1.3 or 2.0 nm runs. (A-C) Relationship between the sum of the proximity indices ($S_{choline}$ + S_{po4} + S_{glycco}) and $V^{Coul}_{lipid\text{-}pept}$ i.e., the Coulombic potential between lipid and peptide. A linear regression model, y = ax + b, where a is the gradient and b is the intercept on the vertical (y) axis derived with the least square fitting is also shown in the following. (A) Gr-Ile_{21}-1-1-1 system (#2). For r=1.3 nm runs, y=-3.18x + 526.70 (p-value=2.03×10^{-8}). For r=2.0 nm runs, y=-1.93x + 1098.33 (p = 4.17×10-10). (B) Gr-IV-1-1-1 system (#7). For r=1.3 nm, y=-2.53x + 826.44 (p=2.74×10^{-8}). For r=2.0 nm, y=-2.07x + 1049.88 (p= 6.32×10^{-6}). (C) Result of the Ch-Ile_{21}-1-1-1 (#9). For r=1.3 nm, y=-3.87x + 817.53 (p=3.50×10^{-10}) and for r=1.6 nm, y=-4.06x + 827.61 (p=2.06×10^{-5}).

	#1	#2 [a]	#6	#7 [a]	#8	#9 [a]
System	**Gr-Ile_{21}-dopc**	**Gr-Ile_{21}-1-1-1**	**Gr-IV-dopc**	**Gr-IV-1-1-1**	**Ch-Ile_{21}-dopc**	**Ch-Ile_{21}-1-1-1**
r (nm)	**1.3**	**1.3**	**1.3**	**1.3**	**1.3**	**1.3**
$V^{LJ}_{lipid\text{-}pept}$ ± SE	-1281.4 ± 13.2	-1279.0 ± 5.3	-1241.6 ± 6.6	-1255.6 ± 9.4	-1071.4 ± 7.3	-1116.5 ± 7.7
{$V^{LJ}_{lipid\text{-}pept}$ (1.3) - $V^{LJ}_{lipid\text{-}pept}$ (2.0)} ± SE	136.2 ± 15.4	119.1 ± 3.9	114.5 ± 6.0	84.6 ± 8.7	78.1 ± 8.1	61.8 ± 7.0
$N_{acyl\text{-}prox}^{dual}$ ± SD, (D_{cutoff}= 5 Å)	0.097 ± 0.309	0.088 ± 0.293	0.065 ± 0.256	0.097 ± 0.306 ($p<10^{-4}$)	0.041 ± 0.210	0.053 ± 0.223 ($p < 0.05$)
$N_{acyl\text{-}dist}^{dual}$± SD, ($D_{cutoff}$= 5 Å)	0.089 ± 0.292	0.170 ± 0.408 ($p<10^{-11}$)	0.108 ± 0.323	0.143 ± 0.368 ($p<10^{-3}$)	0.043 ± 0.205	0.067 ± 0.253 ($p<10^{-3}$)
$N_{acyl\text{-}prox}^{dual}$± SD, ($D_{cutoff}$= 6 Å)	1.106 ± 0.919	1.215 ± 0.939 ($p<10^{-4}$)	0.962 ± 0.868	1.237 ± 0.960 ($p<10^{-28}$)	0.787 ± 0.811	1.011 ± 0.859 ($p<10^{-14}$)
$N_{acyl\text{-}dist}^{dual}$± SD, ($D_{cutoff}$= 6 Å)	1.233 ± 0.934	1.549 ± 0.991 ($p<10^{-17}$)	1.293 ± 0.919	1.470 ± 0.979 ($p<10^{-8}$)	0.746 ± 0.763	1.052 ± 0.855 ($p <10^{-20}$)

[a] p-values based on *t*-test refer to the comparison between the raft-like system and the corresponding DOPC system data. All p-values are shown except for the cases with p>0.05.

Table 4: Lipid chain contacts to peptides in dimeric state.

Intriguingly, in the raft-like bilayers (1:1:1 and 2:1:1), lipid head group atoms also showed trends to have dual contacts with the peptides ($N_{lip\_head\text{-}atom}^{dual}$ of Tables 5 and 6). Thus, in the atomistic simulations, the head group atoms as well as the acyl chain distal segments of the raft-like bilayers were more likely to have dual contacts with both of the dimerized peptides compared to the chains in the non-raft type bilayers.

The lipid-peptide LJ potential energy associates with the number of lipid atoms that have contacts to both peptides

The $V^{LJ}_{lipid\text{-}pept}$, i.e., the lipid-peptide LJ potential energy was shown to contribute to the helix dimer stabilization in the raft-like systems in the above. We have also seen in the above that conformational differences observed in the contact analysis between the raft-like and the non-raft bilayers were seen to associate with the $V^{LJ}_{lipid\text{-}pept}$ term of the potential energy (Table 5). In theory, it is plausible that the lipid atoms with dual contacts will make greater contribution to the $V^{LJ}_{lipid\text{-}pept}$ term (bringing it to a deeply negative value). In support of this, the $V^{LJ}_{lipid\text{-}pept}$ term associated with dually-contacting atoms (Tables 4 and 5), but as within-trajectory correlation (due to slow mixing) tends to increase between-trajectory differences, and it was most likely that this obscured the correlation between $V^{LJ}_{lipid\text{-}pept}$ and the dual contacts count. Intriguingly, when the mean of the 100ns segments of the simulation trajectories were analyzed, $V^{LJ}_{lipid\text{-}pept}$ and dual contacts showed a clear correlation (Figure 6). Thus, the $V^{LJ}_{lipid\text{-}pept}$ potential energy term showed a within-trajectory fluctuation, and such a fluctuation was accompanied by a fluctuation of the count of dual contacts. Together with the decomposition results, this finding suggests an important role for the increased dual contacts in the helix dimer stabilization mediated by the modulation of the lipid-peptide LJ interactions.

Sim ID		**#1**	**#2[a]**	**#3[a]**	**#8**	**#9[a]**
System		**Gr-Ile$_{21}$-dopc**	**Gr-Ile$_{21}$-1-1-1**	**Gr-Ile$_{21}$-2-1-1**	**Ch-Ile$_{21}$-dopc**	**Ch-Ile$_{21}$-1-1-1**
r (nm)		**1.3**	**1.3**	**1.3**	**1.3**	**1.3**
$\{V^{LJ}_{lipid\text{-}pept}(1.3) - V^{LJ}_{lipid\text{-}pept}(2.0)\} \pm SE$		136.2 ± 15.4	119.1 ± 3.9	119.0 ± 8.8	78.1 ± 8.1	61.8 ± 7.0
analyzed group	symbol					
PC head group	$N_{lip\_head\text{-}atom}^{dual} \pm SD$	3.7 ± 3.0	5.0 ± 3.2 ($p<10^{-22}$)	4.9 ± 3.3 ($p<10^{-20}$)	2.2 ± 2.4	2.1 ± 2.3
C2-C6	$N_{lip\_2\text{-}6\text{-}atom}^{dual} \pm SD$	7.9 ± 3.4	7.1 ± 3.3 ($p<10^{-12}$)	7.8 ± 3.8	5.7 ± 3.4	6.1 ± 3.2 ($p<10^{-4}$)
C7-C11	$N_{lip\_7\text{-}11\text{-}atom}^{dual} \pm SD$	7.9 ± 3.4	8.4 ± 3.4 ($p < 10^{-6}$)	8.2 ± 3.4 ($p < 10^{-2}$)	5.9 ± 3.3	6.9 ± 3.3 ($p<10^{-16}$)
C12-C16	$N_{lip\_12\text{-}16\text{-}atom}^{dual} \pm SD$	7.9 ± 3.2	8.5 ± 3.3 ($p<10^{-8}$)	8.3 ± 3.6 ($p<10^{-4}$)	5.7 ± 3.1	6.9 ± 3.2 ($p<10^{-20}$)
cholesterol OH	$N_{lip\_choloh\text{-}atom}^{dual} \pm SD$	-	0.2 ± 0.6	0.2 ± 0.5	-	0.1 ± 0.3
cholesterol carbon	$N_{lip\_cholc\text{-}atom}^{dual} \pm SD$	-	2.2 ± 3.4	2.2 ± 3.6	-	2.1 ± 3.2
total (all lipids)	$N_{lip\_atom}^{dual} \pm SD$	31.3 ± 6.8	32.6 ± 6.9 ($p<10^{-8}$)	32.5 ± 7.0 ($p<10^{-7}$)	22.6 ± 7.2	25.2 ± 6.4 ($p<10^{-20}$)

[a] p-values based on *t*-test refer to the comparison between the raft-like system and the corresponding DOPC system in terms of the phospholipid atom contacts to peptides. All p-values are shown except for the cases with p>0.05.

Table 5: Lipid atom contacts to peptides in dimeric state.

Sim ID		**#6**	**#7[a]**	**#4**	**#5[a]**
System		**Gr-IV-dopc**	**Gr-IV-1-1-1**	**Gr-Ile$_{21}$-popc**	**Gr-Ile$_{21}$-3-1**
r (nm)		**1.3**	**1.3**	**1.3**	**1.3**
$\{V^{LJ}_{lipid\text{-}pept}(1.3) - V^{LJ}_{lipid\text{-}pept}(2.0)\} \pm SE$		114.5 ± 6.0	84.6 ± 8.7	138.9 ± 17.5	133.5 ± 8.1
analyzed group	symbol				

PC head group	$N_{lip\_head\text{-}atom}^{dual} \pm SD$	3.8 ± 2.8	4.2 ± 2.8 ($p < 10^{-6}$)	5.1 ± 3.1	3.8 ± 3.1 ($p < 10^{-22}$)
C2-C6	$N_{lip\_2\text{-}6\text{-}atom}^{dual} \pm SD$	7.0 ± 3.4	6.7 ± 3.5 ($p < 10^{-3}$)	8.1 ± 3.7	6.8 ± 3.4 ($p < 10^{-19}$)
C7-C11	$N_{lip\_7\text{-}11\text{-}atom}^{dual} \pm SD$	8.1 ± 3.3	8.1 ± 3.5	8.2 ± 3.4	7.8 ± 3.4 ($p < 10^{-4}$)
C12-C16	$N_{lip\_12\text{-}16\text{-}atom}^{dual} \pm SD$	7.7 ± 3.1	8.0 ± 3.4 ($p < 10^{-3}$)	8.0 ± 3.3	8.1 ± 3.3
cholesterol OH	$N_{lip\_choloh\text{-}atom}^{dual} \pm SD$	-	0.2 ± 0.6	-	0.2 ± 0.6
cholesterol carbon	$N_{lip\_cholc\text{-}atom}^{dual} \pm SD$	-	3.1 ± 4.2	-	1.9 ± 3.2
total (all lipids)	$N_{lip\_atom}^{dual} \pm SD$	30.0 ± 7.1	31.0 ± 6.8 ($p < 10^{-6}$)	31.0 ± 7.1	30.7 ± 6.8

[a]p-values refer to the *t*-test comparing the cholesterol-containing bilayer system (i.e., #7 and 5) with the corresponding DOPC system (#6 and 4) in the results based on phospholipid atoms. All p-values are shown except for the cases with p>0.05.

Table 6: Lipid atom contacts to dimerized peptides in the IV-peptide simulations and the POPC and 3:1 POPC/cholesterol simulations.

Concluding discussion – both LJ and electrostatic lipid-peptide interactions undergo lipid acyl chain order-associated changes and can jointly modulate helix dimer stability

Our computational analyses showed that increases in saturated FA chains and cholesterol in model membranes shift the monomer-dimer equilibrium of TM helical peptides toward the dimeric state in a sequence-nonspecific manner. This is in agreement with the experiments by Yano et al. [4] that used a similar setting. Our further further analyses focusing on the lipid-peptide contacts showed that different modes of contacts were associated with the membrane-dependent changes in the LJ and electrostatic potential energy profiles [Figure 1F], which are, based on our computation, likely to contribute to the helix dimer stabilization in the raft-like bilayers.

On the other hand, in such settings, UA and AA FFs often yield different dimerization energies [6,7] and such discrepancies may compromise credibility of such computational analyses. In this regard, we note that subtle modifications of the lipid-peptide LJ parameters can cause dramatic changes in the peptide dimerization energy [7]. It is likely that such fine tuning in parameterization is difficult for GROMOS, whose parameterization has been partly guided by the transfer free energy of amino acids side chain analogues from water to apolar solvents, whereas our data showed that such free energies show limited concordance with the helix dimerization energies [data not shown]. To cope with this issue, two approaches may be beneficial. From our experiences, complementary analyses based on AA FFs are useful as our data including Figures 5C and 6C and Tables 3 and 5 showed. Another approach is that readjustment of the UA lipid-peptide LJ parameters based on AA simulation-based reference data, as we previously proposed [7]. In the present study, we chose the standard GROMOS^{53A6}, but we are currently conducting further analyses using modified FFs.

When compared with the LJ interactions, a greater contribution of the electrostatic interactions between phospholipid head groups and the peptide backbone atoms to the helix dimer stabilization was observed (Figure 1B). We also showed that in the DOPC bilayers, an increased number of head groups tend to reside in the proximity of *monomeric* peptides, thereby stabilizing the helix monomers through modulation of the electrostatic interaction between the helices (Tables 2 and 3). Such a monomer-dimer difference was not seen in the raft-like bilayer. However, while we used 21-residue helical peptides similar to the one used in Yano et al. [4], in physiological settings TM helical peptides are normally flanked by polar or charged amino acid residues. Thus, it is not clear to what extent our discussion based on the proximity index can transfer to more physiological settings with flanking sequences. For instance, bending and leaning of choline groups toward the peptides would be affected depending on the flanking sequence, so it is not clear whether the membrane dependency of lipid head group-peptides interaction might be reproduced in the cases with flanking sequences. Further analyses using more physiological systems are necessary to address this issue.

Broadly, the lipid-peptide LJ interaction showed profiles suggestive of a contribution of this term to the helix dimer stabilization in the raft-like bilayers relative to the DOPC bilayer (Figure 1C and [6]). Although this contribution was not large, the scatter plot showed a clear correlation between the dual contact and the lipid-peptide LJ energy (Figure 6) and, together with the increased dual contacts in the raft-like bilayer relative to the DOPC bilayer (Tables 4 and 5), this supports an important contribution of LJ lipid-peptide interaction to the helix dimer stability. Then, it may become of interest to compare the dual contacts with the some structural features of the systems including the peptide orientation. The tilt angle of the peptides with respect to the bilayer normal showed pronounced differences among the bilayers used, with the higher lipid order (based on S_{CD}) leading to smaller tilt angles (Tables 7 and 8). The helix-helix

crossing angle data also exhibited a similar trend when the peptides were held at r=1.3 nm (dimeric state). In this light, the significant correlation observed between the the dual contact count and $V^{LJ}_{lipid\text{-}pept}$ (Figure 6) suggests that the relatively upright orientations and small crossing angles of the peptides facilitate the dual contacts of the lipid molecules in the raft-like bilayers, thereby bringing the $V^{LJ}_{lipid\text{-}pept}$ to a more negative value. Intriguingly, the structural features of the lipid head groups of the raft-like bilayers (1:1:1 and 2:1:1) did not show extended structures based on C-N tilt and C-P tilt (Tables 7 and 8), but they still had greater numbers of dual contacts compared to the non-raft bilayers (Tables 5 and 6). This suggests that the small tilt and crossing angles of the peptides can engender more dual contacts even in the absence of a detectable degree of straightened structures of the lipid head groups.

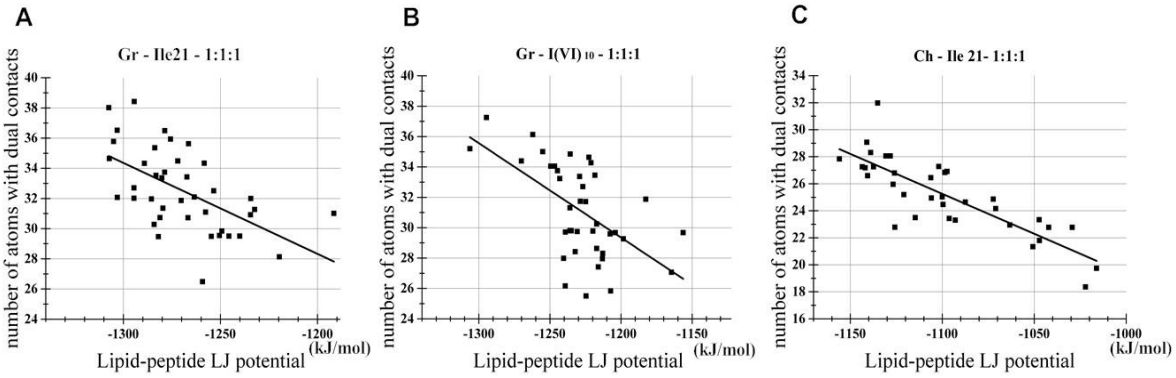

Figure 6: Scatter plot analysis of relationship between the lipid-peptide LJ energy $V^{LJ}_{lipid\text{-}pept}$ and the count of dually-contacting atoms $N_{lip\text{-}atom}{}^{dual}$. Each plot corresponds to a 100ns segment of a simulation trajectory of the r=1.3 nm runs. Line represents the linear regression model, y = ax + b, where a is the gradient and b the intercept on the vertical (y) axis, derived with the least square fitting. (A) Gr-Ile_{21}-1-1-1 (#2). The linear model was y=-0.06 × -44.03 ($p=1.20 \times 10^{-4}$). (b) Gr-IV-1-1-1 (#7). y = -0.06 × -45.23 ($p=1.28 \times 10_{-4}$). (c) Ch-Ile_{21}-1-1-1 (#9). y=-0.06 × -39.83 ($p=1.09 \times 10^{-9}$).

Although it is generally considered that cholesterol straightens out the lipid tails in cholesterol-rich Lo phase lipid bilayer, causing such bilayers to become thicker than Ld phase bilayers [8], it was not likely in our setting that the small peptide tilt and crossing angles in the raft-like bilayers were caused by the hydrophobic mismatches between peptide lengths and the thickness of the hydrophobic core of the membranes for the following reasons. First, the thickness was quite similar between the DOPC and the 1:1:1 bilayers (Table 7) despite the marked difference in peptides tilt and crossing angles. Moreover, both termini of the used peptides lacked polar or charged groups to anchor them to the lipid head groups. Indeed, there was an unappreciable degree of membrane deformation ([6] and data not shown) and we found similar peptide lengths (Ile1 Cα-Ile_{21} Cα distance) among the different bilayers (Tables 7 and 8), suggestive of a negligibly small effect of the negative mismatch.

Sim ID	**#1**		**#3**		**#2**		**#8**		**#9**	
System	**Gr-Ile_{21}-dopc**		**Gr-Ile_{21}-2-1-1**		**Gr-Ile_{21}-1-1-1**		**Ch-Ile_{21}-dopc**		**Ch-Ile_{21}-1-1-1**	
interhelical distance r (nm)	1.3	2.0	1.3	2.0	1.3	2.0	1.3	1.6	1.3	1.6
bilayer thickness based on P-P distance (nm) [a]	4.1 ± 0.1	4.0 ± 0.1	4.3 ± 0.1	4.3 ± 0.1	4.3 ± 0.1	4.3 ± 0.1	3.7 ± 0.5	3.8 ± 0.3	4.3 ± 0.3	4.3 ± 0.3
C-P tilt (degree) [a]	51.2 ± 3.5	48.0 ± 2.8	50.0 ± 2.7	50.0 ± 2.8	50.4 ± 2.7	50.8 ± 2.7	33.1 ± 2.9	33.2 ± 2.9	35.0 ± 2.4	34.8 ± 2.4
C-N tilt (degree) [a]	53.7 ± 2.5	52.2 ± 1.8	52.9 ± 2.0	53.2 ± 2.1	53.3 ± 2.1	52.9 ± 2.1	46.7 ± 2.7	46.7 ± 2.7	47.4 ± 2.3	47.4 ± 2.2
peptide tilt (degree)	17.6 ± 9.6	17.5 ± 9.0	11.9 ± 5.8	13.4 ± 8.1	11.2 ± 5.2	11.5 ± 5.6	24.6 ± 13.1	23.1 ± 13.0	16.1 ± 8.0	18.2 ±

										10.6
helix-helix crossing angle (degree)	26.7 ± 14.0	20.8 ± 11.1	19.3 ± 10.8	19.4 ± 9.9	14.8 ± 7.9	19.6 ± 17.0	22.9 ± 13.9	25.3 ± 17.2	14.0 ± 8.3	19.8 ± 10.4
peptide length (nm) [b]	3.30 ± 0.11	3.36 ± 0.14	3.37 ± 0.10	3.34 ± 0.11	3.38 ± 0.09	3.4 ± 0.1	3.34 ± 0.07	3.35 ± 0.06	3.36 ± 0.06	3.36 ± 0.05
[a] Peptide-containing bilayers were analyzed. [b]The length based on the distance between the Ile1 C_α and Ile21 C_α.										

Table 7: Basic structural properties of the bilayer/peptides systems.

Sim ID	**#6**		**#7**		**#4**		**#5**	
System	**Gr-IV-dopc**		**Gr-IV-1-1-1**		**Gr-Ile$_{21}$-popc**		**Gr-Ile$_{21}$-3-1**	
inter-helical distance r (nm)	1.3	2.0	1.3	2.0	1.3	2.0	1.3	2.0
bilayer thickness based on P-P distance (nm)[a]	4.1 ± 0.1	4.1 ± 0.1	4.3 ± 0.1	4.3 ± 0.1	4.0 ± 0.1	4.0 ± 0.1	4.3 ± 0.1	4.3 ± 0.1
C-P tilt (degree) [a]	53.3 ± 2.5	48.6 ± 2.5	53.5 ± 2.0	50.8 ± 2.5	50.9 ± 3.0	48.0 ± 2.5	50.5 ± 2.6	50.9 ± 2.5
C-N tilt (degree) [a]	52.2 ± 3.1	52.6 ± 1.8	51.6 ± 2.5	53.4 ± 2.0	53.6 ± 2.5	52.6 ± 1.8	53.0 ± 2.0	52.9 ± 2.1
peptide tilt (degree)	15.0 ± 7.6	15.9 ± 7.6	11.0 ± 5.0	11.2 ± 5.0	14.0 ± 6.8	15.8 ± 8.5	12.7 ± 6.2	12.4 ± 5.9
helix-helix crossing angle (degree)	24.6 ± 10.5	22.7 ± 10.3	15.6 ± 7.4	13.3 ± 8.0	20.7 ± 11.5	26.7 ± 10.5	18.4 ± 10.8	17.4 ± 7.8
peptide length (nm)[b]	3.31 ± 0.07	3.33 ± 0.13	3.34 ± 0.08	3.36 ± 0.08	3.28 ± 0.13	3.33 ± 0.13	3.35 ± 0.09	3.37 ± 0.07
[a] Peptide-containing bilayers were analyzed. [b] The length based on the distance between the Ile1 C_α and Ile21 C_α atoms.								

Table 8: Basic structural properties of the bilayer/peptides systems.

The better solvation by ordered lipids observed in this study may provide lipid rafts suitability as a protein clustering platform. Although protein inclusivity is low compared to non-raft microdomains [9], acylation can drive TM proteins into lipid rafts, where TM proteins tend to cluster. In the case of influenza virus that buds from rafts, it is considered that HA protein clusters in lipid rafts to provide a sufficient concentration of HA necessary to mediate efficient virus-cell fusion [10]. Although our comparison between the DOPC and POPC bilayers and that between the POPC and the 3:1 POPC/cholesterol bilayers showed small differences, our findings suggest that such a proposal can be extended to a view that, regardless of residing inside or outside of lipid rafts, the more ordered lipid acyl chains can stabilize the more the dimerization propensity of at least some helical TM proteins. As a consequence of this common principle, the ordered acyl chains of lipid rafts may have provided an advantage in evolution to rafts as platform for clustering as seen in the HA case.

Our observation of the peptide dimer-stabilizing effect of cholesterol and saturated FA is reminiscent of the result by Schneider and coworkers on GpA TM peptide that showed cholesterol dimer-stabilizing effect of 40 mole % cholesterol in various bilayers made up of PC with chains 14:1 to 20:1 [11]. In the latter study, an analysis employing transition temperature the authors showed that acyl chain ordering a key factor stabilizing the GpA TM dimer. However, it should be kept in mind that cholesterol can 'destabilize' the helix dimer in some settings. Matsuzaki and coworkers recently showed that, in a POPC bilayer/$(AALALAA)_3$ model peptide system, a replacement of the central heptad with AGLALGA shows dimer destabilization but changed the cholesterol effect from stabilization to destabilization [12]. The reason why dimer stabilization by cholesterol is not universal is not presently clear, but it is possible that the overall structure of dimerized peptide may affect structural fitness. For example, dimerization mediated by a GxxxG motif and compact dimeric structure may be more sensitive to cholesterol. Besides the presence of flanking sequences, physiological compositions of lipid bilayer may endow distinct features compared to model membranes [13]. Further analysis using

especially of membranes with net charges are also necessary to address these issues.

Conflict of Interest Disclosure

The authors declare no competing financial interest.

References

1. Lange Y, Steck TL (2016) Active membrane cholesterol as a physiological effector. Chem Phys Lipids 199: 74-93.
2. Stangl M, Schneider D (2015) Functional competition within a membrane: lipid recognition *vs.* transmembrane helix oligomerization. Biochimica et Biophysica Acta (BBA)-Biomembranes 1848(9): 1886-1896.
3. Lelimousin M, Limongelli V, Sansom MS (2016) Conformational changes in the epidermal growth factor receptor: Role of the transmembrane domain investigated by coarse-grained metadynamics free energy calculations. JACS 138(33): 10611-10622.
4. Yano Y, Kondo K, Kitani R, et al. (2015) Cholesterol-induced lipophobic interaction between transmembrane helices using ensemble and single-molecule fluorescence resonance energy transfer. Biochemistry 54(6): 1371-1379.
5. Nishizawa M, Nishizawa K (2017) Cholesterol and saturated fatty acid stabilize dimerization of helical transmembrane peptides by lowering energy cost related to peptides desolvation from lipids upon dimerization: An insight from atomistic simulation. Biomed Res Clin Prac 2: 1-8.
6. Nishizawa M, Nishizawa K (2018) Sequence-nonspecific stabilization of transmembrane helical peptide dimer in lipid raft-like bilayers in atomistic simulations. I. Dimerization free energy and impact of lipid-peptide potential energy. Ann Biomed Res 1(1): 105
7. Nishizawa M, Nishizawa K (2016) Free energy of helical transmembrane peptide dimerization in OPLS-AA/Berger force field simulations: inaccuracy and implications for partner-specific Lennard-Jones parameters between peptides and lipids. Molecular Simulation 42(11): 916-926.
8. Yang ST, Kreutzberger, AJ, Lee J, et al. (2016) The role of cholesterol in membrane fusion. Chem Phys Lipids 199: 136-143.
9. Schäfer LV, de Jong DH, Holt A, et al. (2011) Lipid packing drives the segregation of transmembrane helices into disordered lipid domains in model membranes. Proc Natl Acad Sci U S A 108(4): 1343-1348.
10. Takeda M, Leser GP, Russell CJ, et al. (2003) Influenza virus hemagglutinin concentrates in lipid raft microdomains for efficient viral fusion. Proc Natl Acad Sci U. S. A 100(25): 14610-14617.
11. Anbazhagan V, Schneider D (2010) The membrane environment modulates self-association of the human GpA TM domain--implications for membrane protein folding and transmembrane signaling. Biochim Biophys Acta 1798(10): 1899-1907.
12. Yano Y, Furukawa N, Ono S, et al. (2016) Selective amine labeling of cell surface proteins guided by coiled-coil assembly. Biopolymers 106(4): 484-490.
13. Hong H, Bowie JU (2011) Dramatic destabilization of transmembrane helix interactions by features of natural membrane environments. J Am Chem Soc 33(29): 11389-11398.

***Corresponding author:** Kazuhisa Nishizawa, Teikyo University School of Medical Technology, Kaga, Itabashi, Tokyo, 173-8605 Japan, Tel: +81-3-3964-1211, Fax: +81-3-5944-3354; Email: kazunet@med.teikyo-u.ac.jp

Received date: May 04, 2018; **Accepted date:** May 07, 2018; **Published date:** May 09, 2018

Citation: Nishizawa M, Nishizawa K (2018) Sequence-nonspecific Stabilization of Transmembrane Helical Peptide Dimer in Lipid Raft-like Bilayers in Atomistic Simulations. II. Acyl Chain Order-Associated Changes in Lipid-peptide Contacts Concordant with Potential Energy Profiles. *Ann Biomed Res* 1(1): 106.